Sun *et al. Soft Sci* 2022;2:1
DOI: 10.20517/ss.2021.21

Soft Science

Research Article

Open Access

Enhanced electromechanical conversion via in situ grown $CsPbBr_3$ nanoparticle/poly(vinylidene fluoride) fiber composites for physiological signal monitoring

Xindi Sun[1], Fengyuan Zhang[3], Lingyu Zhang[1], Guimin Liu[1], Yalong Wang[1], Yao Wang[1,2], Yuan Deng[2,4]

[1]School of Materials Science and Engineering, Beihang University, Beijing 100191, China.
[2]Hangzhou Innovation Institute, Beihang University, Hangzhou 310052, Zhejiang, China.
[3]Department of Materials Science and Engineering, Southern University of Science and Technology, Shenzhen 518055, Guangdong, China.
[4]Research Institute for Frontier Science, Beihang University, Beijing 100191, China.

Correspondence to: Prof. Yao Wang, School of Materials Science and Engineering, Beihang University, No. 37 Xueyuan Rd., Haidian District, Beijing 100191, China. E-mail: wang-yao@buaa.edu.cn; Prof. Yuan Deng, Hangzhou Innovation Institute, Beihang University, No. 18 Chuanghui Street, Binjiang District, Hangzhou 310052, Zhejiang, China. E-mail: dengyuan@buaa.edu.cn

How to cite this article: Sun X, Zhang F, Zhang L, Liu G, Wang Y, Wang Y, Deng Y. Enhanced electromechanical conversion via in situ grown $CsPbBr_3$ nanoparticle/poly(vinylidene fluoride) fiber composites for physiological signal monitoring. *Soft Sci* 2022;2:1. https://dx.doi.org/10.20517/ss.2021.21

Received: 26 Dec 2021 **First Decision:** 17 Jan 2022 **Revised:** 20 Jan 2022 **Accepted:** 24 Jan 2022 **Published:** 29 Jan 2022

Academic Editor: Zhifeng Ren **Copy Editor:** Xi-Jun Chen **Production Editor:** Xi-Jun Chen

Abstract

Mechanical energy conversion based on the piezoelectric principle has received significant attention due to its promising applications in sustainable power supply systems and sensor technology. Ferroelectric poly(vinylidene fluoride) (PVDF) combines the advantages of both good electromechanical coupling and easy processability, yet its low piezoelectric coefficient limits its output performance and it thus cannot meet the increasing requirements for power generation and sensing. Here, inorganic metal halide perovskite $CsPbBr_3$ (CPB) nanoparticles are incorporated into PVDF fibers via an electrospinning technique, where an *in situ* crystallization and growth process of the CPB nanoparticles is established. Both the CPB nanoparticles and PVDF fibers are poled by the electric field during the electrospinning process, which promotes the formation of the polar phase of PVDF and distortion of the CPB lattice, resulting in greatly enhanced piezoelectric performance for the CPB/PVDF composites. The output performance under the external force of a flexible generator developed from electrospun CPB/PVDF films is significantly enhanced compared with the neat PVDF film, with an 8.4 times higher maximum open circuit voltage value. Furthermore, the measurements on the microscopic piezoelectric responses unambiguously reveal that the increased polar phase mainly contributes to the enhanced electromechanical coupling. The functions of the CPB/PVDF films as physiological signal monitoring sensors are determined and they demonstrate their potential

© The Author(s) 2022. **Open Access** This article is licensed under a Creative Commons Attribution 4.0 International License (https://creativecommons.org/licenses/by/4.0/), which permits unrestricted use, sharing, adaptation, distribution and reproduction in any medium or format, for any purpose, even commercially, as long as you give appropriate credit to the original author(s) and the source, provide a link to the Creative Commons license, and indicate if changes were made.

applications as flexible piezoelectric generators and electronics for wearable health monitoring.

Keywords: Electromechanical conversion, PVDF fibers, inorganic metal halide perovskite, physiological signal monitoring

INTRODUCTION

With the flourishing of technologies based on the Internet of Things, distributed power supply systems that are portable, wearable, thin, lightweight and have long operating lifetimes or are even maintenance-free are urgently required for various electronics[1,2]. Energy harvesting from the environment is an ideal solution and has been extensively studied in recent years[3-6]. The main energy conversion principles include the piezoelectric[7] and triboelectric effects[8], which convert mechanical energy into electrical energy, the thermoelectric[9] and pyroelectric effects[10], which convert thermal energy into electrical energy, and the photovoltaic effect[11], which converts solar energy into electrical energy.

Among these effects, transducers based on the piezoelectric effect have been developed based on piezoelectric ceramics over many years and have been widely used as actuators, ultrasonic motors, resonators, sonar detectors and so on[12]. The piezoelectric coefficient d_{ij} is a (3 × 6) tensor and the common two elements in most piezoelectric materials are d_{31} and d_{33}. These correspond to two transduction mechanisms and transducer working modes, i.e., the voltage generated in a direction perpendicular to or in the same direction of the applied stress for the 31 and 33 modes, respectively.

Ferroelectric polymers, typically poly(vinylidene fluoride) (PVDF) and its copolymer poly(vinylidene fluoride-*co*-trifluoride ethylene), combine the advantages of both good electromechanical coupling and easy processability. As a result, they have received considerable attention in mechanical energy harvesting from various types of vibrations and pressure, with unique advantages in power generators for wearable electronics that harvest energy from human movements[13-15]. Nevertheless, the low piezoelectric coefficients of these polymers, i.e., generally below 30 pm/V, have impeded their applications as high-power generators and high-sensitivity strain/stress sensors. A general strategy is to encapsulate strong piezoelectric ceramic materials, such as $Pb(Zr,Ti)O_3$, $BaTiO_3$, $(K,Na)NbO_3$ and $(Na_{1/2}Bi_{1/2})TiO_3$-$BaTiO_3$[16-20], to form composites to enhance the electromechanical conversion capability. However, this also causes a rise in the modulus of the composites, accompanied by an increase in rigidity, and therefore requires a high voltage to polarize the samples to show macroscopic piezoelectricity.

Metal halide perovskites, with the chemical formula ABX_3, where A is a monovalent cation, such as $(CH_3NH_3)^+$ (MA), $CH_3(NH_2)_2^+$ (FA), Cs^+ or Rb^+, B is a divalent metal cation, such as Pb^{2+} or Sn^{2+}, and X is a monovalent halogen anion, such as I^-, Cl^- or Br^-, have emerged as exceptional material systems that possess rich physical features, including excellent optoelectronic properties[21,22]. In addition, they also show some dielectric phenomena related to their polar phase, such as the characteristic of a ferroelastic electret, where a spontaneous lattice strain is coupled to long-lived metastable polarization states[23]. This strongly suggests that halide perovskites are good candidates as fillers to boost the electromechanical coupling of ferroelectric polymers to enable high-performance mechanical energy harvesting. Furthermore, halide perovskites also generally have a magnitude lower Young's modulus i.e., around a dozen GPa[24], than piezoelectric ceramics, which is very beneficial for flexible electronics. Several research groups have already made attempts to fabricate polymer-based nanocomposites that incorporate metal halide perovskites, for example, $FAPbBr_3$/PVDF[25], $MAPbI_3$/PVDF[26] and $FAPbBr_3$/polydimethylsiloxane[27]. The piezoelectric generators developed based on these composites show significant enhancements in output voltage and current density compared to those made from only polymers, thereby demonstrating their promising potential as nanogenerators and sensors.

Compared to hybrid halide perovskites, where the A site ion is MA^+ or FA^+, all inorganic perovskites, such as $CsPbBr_3$, are more stable[11]. Recently, Kim *et al.*[28] reported a high piezoelectric coefficient of d_{33} ~40.3 pm/V, which was experimentally obtained for $CsPbBr_3$ through a poling process. This enhanced piezoelectricity is related to the distortion of the $PbBr_6$ octahedron under poling[28], indicating that a further enhancement in piezoelectricity could be achieved via a proper poling process for perovskite/polymer composites. Here, we demonstrate that an enhanced electromechanical conversion performance can be accomplished via the use of *in situ* grown $CsPbBr_3$ (CPB) nanoparticles encapsulated in PVDF fibers by employing an electrospinning technique, during which both the PVDF fibers and CPB are poled for higher piezoelectricity. In addition, the crystallization and growth of CPB nanoparticles are confined within the polymer chains and subjected to the poling effect from the electric field, thereby generating unique composite microstructures. The devices developed from CPB/PVDF nanocomposite films function effectively as electronics for wearable physiological signal monitoring.

EXPERIMENTAL

Materials

Lead (II) bromide ($PbBr_2$, 99.0%) and cesium bromide (CsBr, 99.9%) were provided by Aladdin Industrial Corporation. PVDF powder was supplied by 3F Co., Ltd. (Shanghai, China). N,N-dimethylformamide (DMF) was purchased from Sinopharm Chemical Reagent Co., Ltd. All the chemicals and reagents were used as received without further purification.

Preparation of CPB/PVDF nanocomposite fiber films

$PbBr_2$ and CsBr with a mass ratio of 7:4 were dissolved in 10 mL of DMF and 6.67 mL of acetone. The mixture was then stirred at 45 °C for 30 min for complete dissolution to form an orange transparent solution. Subsequently, 2.2 g of PVDF were added to the solution and it was stirred constantly for 24 h. The weight fractions of $CsPbBr_3$, increasing from 1 to 6 wt.%, with respect to the total mass of the mixture were designed for the nanocomposite composition. The mixed precursor was loaded into a 10 mL syringe attached to a 23 G stainless steel needle. A high voltage power of 18 kV was applied between the needle and a roller wrapped in aluminum foil. The distance between the needle and the collector was ~15 cm. The feed speed was 7 μL/min and the rotation speed was 600 rpm/min. The whole electrospinning process was maintained at 26 °C with humidity below 20% RH. Finally, the collected fibers were removed from the aluminum foil and dried in a vacuum for 24 h.

Fabrication of physiological signal sensors

The as-electrospun fibers were sandwiched between polyimide films and pressed at 45 °C for 8 h to form compact films. The fiber films were then cut into the desired shape for various devices and Cu electrodes in various patterns were sputtered via masks. Wires were then connected via silver paste.

Characterization

Scanning electron microscopy (SUPRA55, FEI, Carl Zeiss) was used to record the topographic images of the nanocomposite fiber films and the cross-sectional image of the nanogenerator. Transmission electron microscopy (TEM, JEM-2100F, JEOL) was used to observe the morphologies of the CPB/PVDF fibers. The crystalline phase of the CPB/PVDF nanocomposite fibers was characterized by combining X-ray diffraction (XRD, D/Max 2200/PC) with Cu K_α radiation (λ = 1.54 Å) at a scanning rate of 4°/min in the 2θ range from 10° to 50° and Fourier transform infrared spectroscopy (FTIR, Nicolet 6700, ThermoFisher). Differential scanning calorimetry (DSC, STA-449F3, NETZSCH) was carried out under a N_2 atmosphere with a temperature rising rate of 10 °C/min to study the crystallization behavior of the composites. Ultraviolet-visible absorption (UV-vis) spectra were collected from a UV-3600 spectrophotometer from Shimadzu. The photoluminescence (PL) spectra of the CPB/PVDF nanocomposites were measured by a Hitachi F-7000 fluorescence spectrophotometer. Piezoresponse force microscopy (PFM, Cypher ES, Asylum Research) was employed to measure the piezoelectric response of the nanocomposites. The Pt-coated probes (Arrow CONTPt, k ~0.2 N/m, NanoWorld) were used for recording the PFM images.

Electromechanical conversion measurements

A step motor (LinMot, E1100) was used to provide different normal mechanical forces. An oscilloscope (Tektronix TBS 2102) was used to detect the output voltage of the devices upon bending and mechanical compression, while a low-noise current preamplifier (Stanford Research SR570) was used to collect the current signals of the sensors for pulse wave and pronunciation monitoring.

RESULTS AND DISCUSSION

During the electrospinning process, the crystallization of CPB was finished *in situ* in the polymer forming CPB/PVDF nanocomposite fibers. The microstructures of the as-electrospun nanocomposite fibers were observed via TEM, as shown in Figure 1A-D, with the CPB content increasing from 3 to 6 wt.%. As shown in Figure 1A, at a low CPB concentration, the CPB fillers are mainly in the form of small nanoparticles with sizes of ~6-8 nm and are randomly distributed in the PVDF fiber matrix. As the CPB concentration increases, the particles begin to aggregate aligned along the electric field direction applied during the electrospinning process, as clearly shown in Figure 1B. As the CPB concentration further increases to 5 and 6 wt.%, these small nanoparticles grow larger along the electric field direction [Figure 1C], and finally, some nanoparticles grow into one-dimensional (1D) nanorods with lengths of ~30-40 nm, as presented in Figure 1D.

A schematic illustration of the *in situ* nucleation of CPB in the PVDF polymer fiber process is illustrated in Figure 1E. In the precursor mixture, the CPB nuclei are wrapped by polymer chains, as the precursor is sprayed under a high voltage, and the formation of the PVDF fiber and the *in situ* nucleation of CPB crystals proceed simultaneously as the solvent evaporates. Due to the confined volume provided by PVDF chains, the crystal growth for CPB nanoparticles is limited. Owing to the existence of the high voltage, both the CPB and PVDF are poled, causing the appearance of partial charges, and as the CPB concentration increases, the charged particles prefer to aggregate aligned along the extended chain direction induced by the electric field and gradually grow into nanorods.

Since the as-electrospun fiber films have poor mechanical strength, all the CPB/PVDF nanocomposite fiber films were hot-pressed to increase the mechanical strength. The morphologies of the as-electrospun fibers and hot-pressed films are shown in Supplementary Figure 1A and B. The corresponding diameter distribution of the fibers before and after hot pressing is presented in Supplementary Figure 1C and D, respectively. Hot pressing condenses the electrospun fibers and the fiber size slightly increases from 1.0 μm with a large scattering distribution to uniformity at 1.3 μm. The representative cross-sectional image of the CPB/PVDF fiber film further demonstrates the uniformly distributed fibers in Supplementary Figure 1E.

The crystalline phases of the CPB/PVDF fiber films were examined by combining XRD and FTIR analysis. As shown in Figure 2A, CPB crystallized in the pure perovskite structure with an orthorhombic phase (PDF card #18-0364) and with increasing CPB content, the diffraction intensity of the perovskite phase increases when the CPB content up to 5 wt.%, with a further increase in CPB content resulting in low crystallinity of the CPB crystals. Calculations of the crystal lattice parameters of CPB nanoparticles in various content

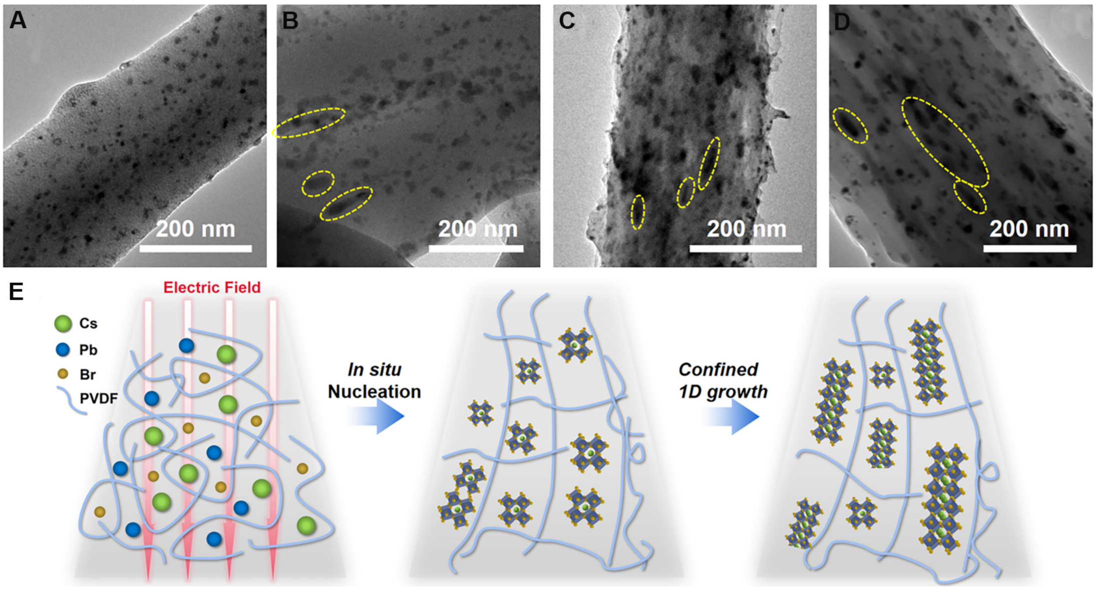

Figure 1. (A-D) TEM images of a single CPB/PVDF nanocomposite fiber with increasing CPB weight fraction: (A) 3 wt.%; (B) 4 wt.%; (C) 5 wt.%; (D) 6 wt.%. The dash circles indicate the CPB nanorods. (E) Schematic illustration on the *in situ* growth mechanism of CPB from nanoparticles to 1D nanorods. CPB: $CsPbBr_3$; PVDF: poly(vinylidene fluoride).

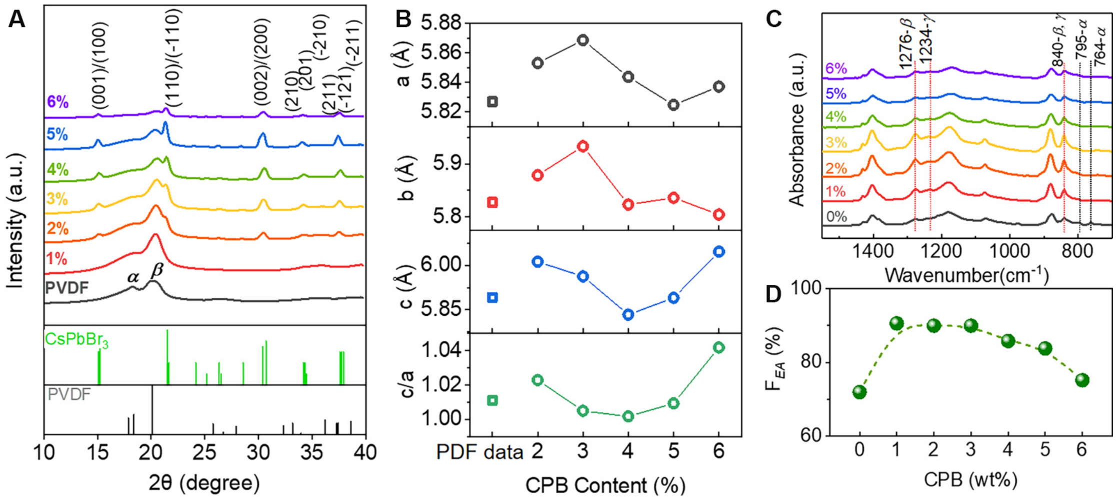

Figure 2. (A) XRD patterns of CPB/PVDF nanocomposite fiber films with CPB loadings from 0 to 6 wt.%. (B) Variation of crystal lattice parameters with CPB content. Diffraction data from standard PDF cards (CPB: #18-0364, PVDF: #42-1649) are depicted for indexing and comparison. (C) FTIR spectra of CPB/PVDF nanocomposite fiber films with increasing CPB loadings from 0 to 6 wt.%. (D) Variation of electroactive phase fraction with the content of CPB nanoparticles. CPB: $CsPbBr_3$; PVDF: poly(vinylidene fluoride); FTIR: Fourier transform infrared spectroscopy.

CPB/PVDF nanocomposites are presented in Figure 2B. A clear crystal lattice distortion of the CPB nanoparticles during the nucleation process under an electric field was observed. The CPB nanoparticles are compressed gradually along the *c*-axis with a CPB content increasing to 4 wt.%, with a further increase in the CPB content results in expansion along the *c*-axis. While the pure PVDF film crystallized in both the α and β phases, when the CPB nanoparticles are incorporated, the ferroelectric β phase becomes dominant. More detailed information on the phase evolution of PVDF could be revealed from the FTIR spectra, as shown in Figure 2C.

As seen from the infrared intensity evolution of characteristic peaks for the β phase at 840 and 1276 cm^{-1}, it is found that a low CPB concentration (below 4 wt.%) results in a higher β phase fraction (F_{EA}), which could be estimated from the De Gregorio equation:

$$F_{\mathrm{EA}}=\frac{I_{EA}}{\left(\frac{K_{EA}}{K_{a}}\right)I_{\alpha}+I_{EA}}\times 100\% \tag{1}$$

where $I_{\boxtimes}$ and I_{EA} are the absorbance intensities at 764 and 840 cm^{-1}, respectively, K_{EA} and $K_{\boxtimes}$ are the absorption coefficients at the corresponding wavenumber, with values of 6.1×10^4 and 7.7×10^4 cm^2·mol^{-1}, respectively. The calculation of the variation of the β phase fraction with the CPB content is summarized in Figure 2D, showing that F_{EA} could be enhanced from 72% to 90%, and further increase in CPB does not result in higher F_{EA}. Since incorporating CPB also influences the crystallinity of PVDF matrix and thus will affect the F_{EA} value, the variation on the crystallinity of the composite with respect to the CPB content is calculated from the DSC curves (shown in Supplementary Figure 2A) according to:

$$\chi_c=\frac{\Delta H_f}{(1 - \phi)\Delta H_m{}^{100}} \tag{2}$$

where ΔH_f is the melting enthalpy of the CPB/PVDF nanocomposite, ϕ is the mass ratio of CPB nanoparticles in the composite and $\Delta H_m{}^{100}$ is the melting enthalpy of a 100% crystalline PVDF ($\Delta H_m{}^{100}$ = 104.6 J/g[29]). As presented in Supplementary Figure 2B, a higher CPB content results in lower polymer crystallinity, thus the F_{EA} falls at high CPB contents.

The CPB perovskite has intrinsic outstanding luminescence properties and when incorporating into the PVDF fiber matrix, the nanocomposites also exhibit strong luminescence, as shown in Figure 3. The PL peaks for all the CPB/PVDF nanocomposites are centered at ~518 nm with a slight shift to 520 nm at high CPB contents. Meanwhile, the absorption peaks for CPB contents lower than 4 wt.% are located at 507-510 nm, with a Stokes shift of 8-11 nm between the absorption and photoluminescence peaks observed. When the CPB content exceeds 4 wt.%, the absorption peak shifts to 513-516 nm with a decreased Stokes shift to 4-5 nm. The Stokes shift in CPB nanocrystals has been revealed to be related to the variation in nanoparticle size[30], which is consistent with the morphology transition from zero-dimensional nanoparticles to 1D nanorods. Compared to conventional piezoelectrics, halide perovskites endow an additional photoluminescence function to the polymer-based mechanical energy harvesters, which have potential applications for multifunctional devices.

The electromechanical conversion performance of the devices made from a series of CPB/PVDF nanocomposite fiber films was examined by monitoring the voltage output upon applying various cyclic normal forces, i.e., 10, 15, 20 and 25 N, respectively, at a fixed frequency of 2 Hz, with the data shown in Figure 4A-G. The variations in the maximum output at each CPB content measured at the same forces are summarized in Figure 4H. Generally, the output voltage increases with increasing applied forces and also increases with CPB content until 4 wt.%, at which the maximum output voltage was achieved with ~90 V at 25 N (peak-to-peak). Based on the piezoelectric conversion, the open circuit voltage is expressed as:

$$V_{oc}=\frac{d_{ij}}{\varepsilon_0\varepsilon_r}\sigma_{ij}t \tag{3}$$

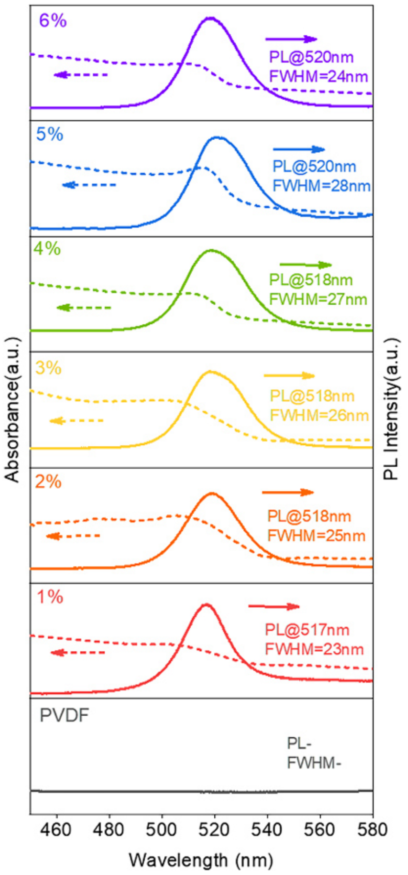

Figure 3. UV-vis absorption and PL emission spectra of CPB/PVDF nanocomposite fiber films with increasing CPB loadings from 0 to 6 wt.%. UV-vis: Ultraviolet-visible; PL: photoluminescence; CPB: $CsPbBr_3$; PVDF: poly(vinylidene fluoride).

where σ_{ij} is the applied stress, d_{ij} is the piezoelectric coefficient, t is the thickness of the piezoelectric material along the stress direction and ε_0 and ε_r are the permittivity of a vacuum and the relative dielectric constant, respectively. Here, the test was carried out in the 33 mode and in order to exclude the variation of V_{oc} brought by film thickness, the normalized output voltages with respect to film thickness are shown in Figure 4I for better comparison. The 4 wt.% CPB/PVDF film shows significantly higher electromechanical conversion ability than the rest of the films, i.e., 8.4 times higher than the neat PVDF film and 1.8 times higher than the 5 wt.% CPB/PVDF film, probably due to an optimal value resulted from high piezoelectric coefficient d_{33} and moderate dielectric constant 9.8@1 kHz[31] according to Equation 3. Upon finger tapping (stress around 4.75 kPa), the 4 wt.% CPB/PVDF film could output an open-circuit voltage of 13 V and a short-circuit current of 1.3 μA, as shown in Figure 4J.

The electromechanical conversion performance of the *in situ* grown CPB/PVDF nanocomposite fiber films developed here was compared with recently reported perovskite/polymer composite-based nanogenerators, as summarized in Table 1. These results reveal that the CPB/PVDF nanocomposite fiber films show quite competitive electromechanical conversion performance with high V_{oc} obtained under moderate stress (dozens of kPa, much lower than the widely reported ~MPa magnitude).

To gain an understanding of the microstructural mechanism of enhanced electromechanical conversion in CPB/PVDF composite fiber films, dual-AC resonance-tracking PFM measurements have been employed[38].

Table 1. Comparison of output performance between recent studies and this work

Perovskites	Polymer	Output performances	Ref.
$MASnI_3$	Porous PVDF	12 V, 4 μA/cm^2 @ 0.5 MPa	[32]
$FASnI_3$	PVDF	23 V, 35 mW/cm^2 @ 0.1 MPa	[33]
$MAPbI_3$	PVDF	220 mV @7.5 N, 4 Hz	[34]
$MAPbI_3$	PVDF	0.107 V/kPa	[35]
$FAPbBr_2I$	Porous PVDF	85 V, 30 μA (peak to peak) @30 Hz	[36]
$CsPbBr_3$	PVDF	120 V, 35 μA @100 MPa	[37]
$CsPbBr_3$	PVDF fiber	90 V (peak to peak) @62.5 kPa, 2 Hz 13 V, 1.3 μA @finger tapping	This work

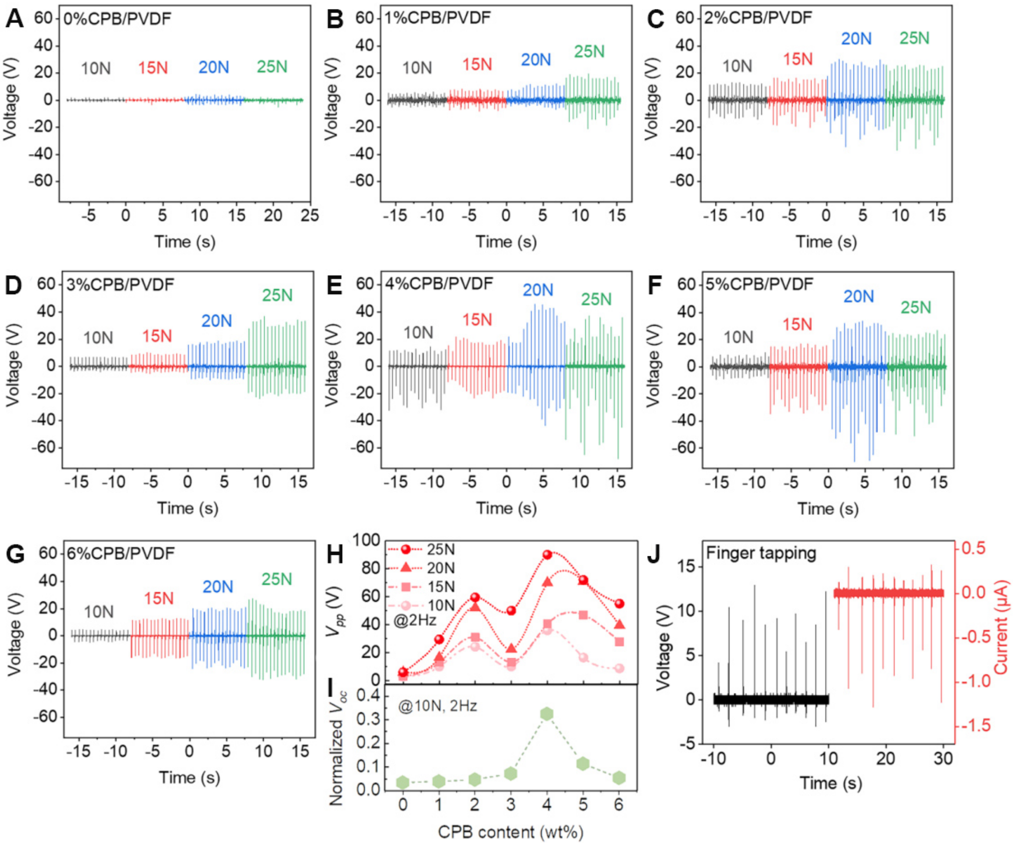

Figure 4. (A-G) Cyclic voltage output performances of CPB/PVDF nanocomposite fiber films with increasing CPB loadings from 0 to 6 wt.% under various applied forces of 10, 15, 20 and 25 N, respectively, measured at 2 Hz. (H) Comparison on variation of maximum output voltage (peak-to-peak) with CPB loadings under fixed force. (I) Normalized maximum output voltage with respect to film thicknesses measured at 10 N, 2 Hz. (J) Simultaneously collected *Voc* and short-circuit current signals upon finger tapping the 4 wt.% CPB/PVDF device repeatedly. CPB: $CsPbBr_3$; PVDF: poly(vinylidene fluoride).

Topographical images of the PVDF and CPB/PVDF fibers are shown in Figure 5A and E, respectively. The corresponding vertical and lateral amplitude signal mappings of PVDF and CPB/PVDF nanocomposite fibers are shown in Figure 5B, C, F and G, respectively. As seen, for the pure PVDF fiber, piezoelectric responses are weak over the whole scanned area in both vertical and lateral orientations, with scattered moderate vertical responses from the areas surrounding fiber/fiber interfaces. In stark contrast, strong piezoelectric responses are obtained on the whole CPB/PVDF fibers from vertical orientation and also some polarization components lie in the plane direction so that strong piezoelectric responses are observed from

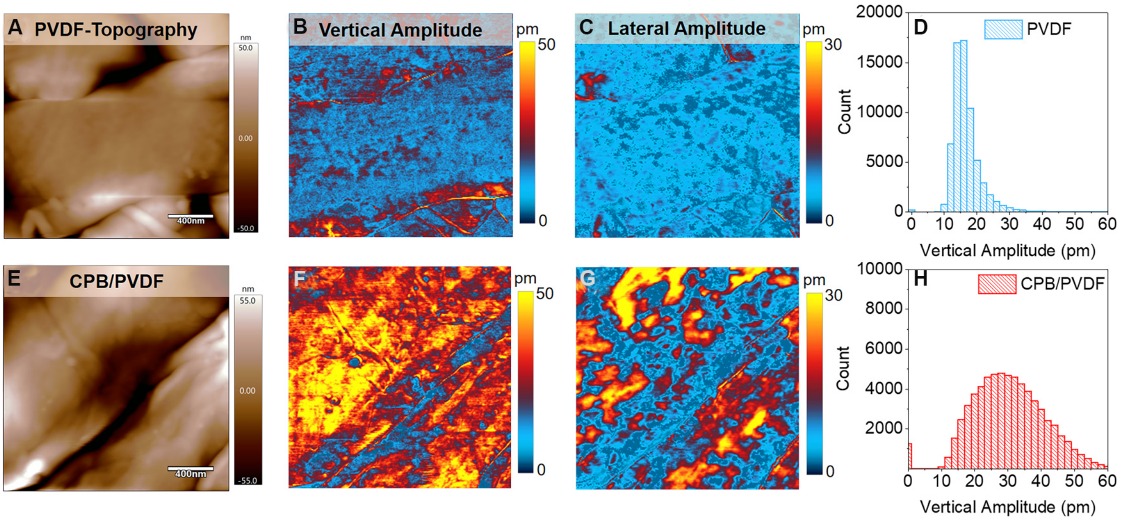

Figure 5. PFM measurements of the piezoelectric responses of (A-D) PVDF and (E-H) CPB/PVDF nanocomposite fiber films at a 4 wt.% CPB loading. (A, E) Topographic images of films. (B, F) Corresponding vertical amplitude and (C, G) lateral amplitude piezoelectric responses obtained at an *ac* voltage of 5 V of the same area shown in (A, E). (D, H) Piezoelectric response histograms from vertical amplitude values. The scan area is 2 × 2 μm^2.

lateral amplitude signals. Frequency images captured simultaneously with the vertical amplitude images are provided in Supplementary Figure 3 to prove that the contact resonance frequency was successfully tracked in most points (higher than 98%) during the scanning, indicating high reliability of the piezoelectric responses obtained here. Histograms of vertical amplitude signals are summarized in Figure 5D and H for the PVDF and CPB/PVDF nanocomposite fibers, respectively. The response distribution for PVDF is within a narrow range, from 10-30 pm and centered at ~15 pm, while the responses for CPB/PVDF show a wide distribution from 20 to 60 pm, with the center at ~30 pm, which is at least double the value of that for the PVDF fiber. The PFM results strongly support the contribution from the increased polar phase to the significant enhancement in electromechanical conversion in the CPB/PVDF nanocomposite.

The functionalities of the devices integrated from the CPB/PVDF nanocomposite fiber films for physiological signal monitoring are demonstrated in Figure 6. A 1 × 3 sensor array was attached tightly to the wrist of the tester to read the pulse wave from the positions of Cun, Guan and Chi, respectively, as shown in the inset of Figure 6A, which mimics the diagnosis process of the traditional Chinese physician feeling the pulse palpation. Pulse wave signals collected from three positions show distinctive waves characteristics and gender difference, reflecting relevant health information. The sensor is capable of differentiating pronunciation of the words with various number of syllables via perceiving the vocal vibration when attached to human throat. As shown in Figure 6B, when a speaker said three words "Ah", "Cindy", and "Sivona", respectively, three different characteristic waveforms were obtained. One strong peak appeared for the monosyllabic word "Ah", two peaks with one weak and one strong for the disyllabic word "Cindy" whose accent is on the second syllable, and three peaks with one weak and two strong ones for the trisyllabic word "Sivona" whose accent is on the last two syllables. Two sensors were attached to the finger joint to monitor their movement simultaneously. As shown in Figure 6C, the individual bending of a single finger and simultaneous bending of both fingers could be timely and accurately recorded from two individual channels.

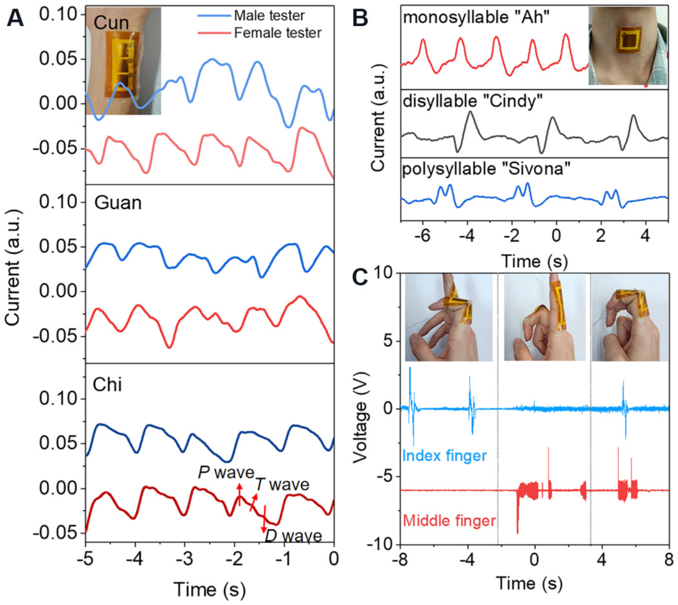

Figure 6. Physiological signal monitoring functionalities of wearable sensors developed using CPB/PVDF fiber films. (A) Pulse waves of female and male testers measured employing a 1 × 3 sensor array to monitor pulses from locations called Cun, Guan and Chi, respectively. (B) Monitoring on vocal fold vibration pronouncing words with various number of syllables. (C) Simultaneous output of two sensors attached to index finger and middle finger with different gestures, respectively. The insets show the images of sensors at work.

CONCLUSIONS

In summary, CPB/PVDF fiber films have been fabricated via an electrospinning technique, where the CPB nanoparticles were crystallized and grown confined within the PVDF chains. In the meantime, both the CPB nanoparticles and PVDF fibers were poled by the electric field, resulting in a greatly enhanced piezoelectric performance. The output performance of the CPB/PVDF films was boosted significantly over neat PVDF film, i.e., with the maximum value enhanced 8.4 times. PFM measurements unambiguously reveal that the enhanced electromechanical coupling originates from the increased polar phase with strong piezoelectric response. The precise and sensitive sensing functionalities of CPB/PVDF film-based device on pulse wave and body movements explicitly demonstrate its potential applications as flexible piezoelectric generators and wearable health monitoring electronics.

DECLARATIONS

Authors' contributions

Conception and design of the study: Wang Y
Performed data analysis and interpretation: Sun X, Wang Y
Performed data acquisition: Sun X, Zhang F, Zhang L, Liu G, Wang Y
Provided administrative, technical, and material support: Wang Y, Deng Y

Availability of data and materials

Correspondence and requests for data and materials should be addressed to Wang Y.

Financial support and sponsorship

This work was supported by National Natural Science Foundation of China (Grant No. 51872009, 92066203), Guangdong Basic and Applied Basic Research Foundation (2021A1515110155) and the Fundamental Research Funds for the Central Universities.

Conflicts of interest
All authors declared that there are no conflicts of interest.

Ethical approval and consent to participate
This study involved the non-invasive use of skin-mounted wearable sensors to collect physiological signals. All procedures were externally applied, did not involve skin penetration, and posed no physical or psychological risk to participants. Therefore, the study met the criteria for exemption from formal ethical review. All participants provided informed consent prior to their participation.

Consent for publication
Not applicable.

Copyright
© The Author(s) 2022.

REFERENCES

1. Ryu H, Yoon HJ, Kim SW. Hybrid energy harvesters: toward sustainable energy harvesting. *Adv Mater* 2019;31:e1802898. DOI PubMed
2. Gao M, Wang P, Jiang L, et al. Power generation for wearable systems. *Energy Environ Sci* 2021;14:2114-57. DOI
3. Peng B, Zhao F, Ping J, Ying Y. Recent advances in nanomaterial-enabled wearable sensors: material synthesis, sensor design, and personal health monitoring. *Small* 2020;16:e2002681. DOI PubMed
4. Vallem V, Sargolzaeiaval Y, Ozturk M, Lai YC, Dickey MD. Energy harvesting and storage with soft and stretchable materials. *Adv Mater* 2021;33:e2004832. DOI PubMed
5. Qin Y, Wang X, Wang ZL. Erratum: microfibre-nanowire hybrid structure for energy scavenging. *Nature* 2009;457:340-340. DOI
6. Chandrasekaran S, Bowen C, Roscow J, et al. Micro-scale to nano-scale generators for energy harvesting: self powered piezoelectric, triboelectric and hybrid devices. *Phys Rep* 2019;792:1-33. DOI
7. Haertling GH. Ferroelectric ceramics: history and technology. *J Am Ceram Soc* 1999;82:797-818. DOI
8. Fan FR, Tang W, Wang ZL. Flexible nanogenerators for energy harvesting and self-powered electronics. *Adv Mater* 2016;28:4283-305. DOI PubMed
9. He J, Tritt TM. Advances in thermoelectric materials research: looking back and moving forward. *Science* 2017;357:eaak9997. DOI PubMed
10. Bowen CR, Taylor J, Leboulbar E, Zabek D, Chauhan A, Vaish R. Pyroelectric materials and devices for energy harvesting applications. *Energy Environ Sci* 2014;7:3836-56. DOI
11. Kovalenko MV, Protesescu L, Bodnarchuk MI. Properties and potential optoelectronic applications of lead halide perovskite nanocrystals. *Science* 2017;358:745-50. DOI PubMed
12. Anton SR, Sodano HA. A review of power harvesting using piezoelectric materials (2003-2006). *Smart Mater Struct* 2007;16:R1-R21. DOI
13. Martins P, Lopes A, Lanceros-mendez S. Electroactive phases of poly(vinylidene fluoride): determination, processing and applications. *Prog Polym Sci* 2014;39:683-706. DOI
14. Shepelin NA, Glushenkov AM, Lussini VC, et al. New developments in composites, copolymer technologies and processing techniques for flexible fluoropolymer piezoelectric generators for efficient energy harvesting. *Energy Environ Sci* 2019;12:1143-76. DOI
15. Wei H, Wang H, Xia Y, et al. An overview of lead-free piezoelectric materials and devices. *J Mater Chem C* 2018;6:12446-67. DOI
16. Chen X, Li X, Shao J, et al. High-performance piezoelectric nanogenerators with imprinted P(VDF-TrFE)/$BaTiO_3$ nanocomposite micropillars for self-powered flexible sensors. *Small* 2017;13:1604245. DOI PubMed
17. Kim K, Zhu W, Qu X, et al. 3D optical printing of piezoelectric nanoparticle-polymer composite materials. *ACS Nano* 2014;8:9799-806. DOI PubMed
18. Jain A, K. J. P, Sharma AK, Jain A, Rashmi PN. Dielectric and piezoelectric properties of PVDF/PZT composites: a review. *Polym Eng Sci* 2015;55:1589-616. DOI
19. Saito Y, Takao H, Tani T, et al. Lead-free piezoceramics. *Nature* 2004;432:84-7. DOI PubMed
20. Liu B, Lu B, Chen X, et al. A high-performance flexible piezoelectric energy harvester based on lead-free $(Na_{0\cdot5}Bi_{0\cdot5})TiO_3$-$BaTiO_3$ piezoelectric nanofibers. *J Mater Chem A* 2017;5:23634-40. DOI PubMed
21. Green MA, Ho-baillie A, Snaith HJ. The emergence of perovskite solar cells. *Nature Photon* 2014;8:506-14. DOI

22. Stranks SD, Snaith HJ. Metal-halide perovskites for photovoltaic and light-emitting devices. *Nat Nanotechnol* 2015;10:391-402. DOI PubMed
23. Wilson JN, Frost JM, Wallace SK, Walsh A. Dielectric and ferroic properties of metal halide perovskites. *APL Materials* 2019;7:010901. DOI
24. Rakita Y, Cohen SR, Kedem NK, Hodes G, Cahen D. Mechanical properties of APbX3 (A = Cs or CH3NH3; X= I or Br) perovskite single crystals. *MRS Commun* 2015;5:623-9. DOI
25. Ding R, Zhang X, Chen G, et al. High-performance piezoelectric nanogenerators composed of formamidinium lead halide perovskite nanoparticles and poly(vinylidene fluoride). *Nano Energy* 2017;37:126-35. DOI
26. Tusiime R, Zabihi F, Tebyetekerwa M, et al. High stress-driven voltages in net-like layer-supported organic-inorganic perovskites. *J Mater Chem C* 2020;8:2643-58. DOI
27. Ding R, Liu H, Zhang X, et al. Flexible piezoelectric nanocomposite generators based on formamidinium lead halide perovskite nanoparticles. *Adv Funct Mater* 2016;26:7708-16. DOI
28. Kim DB, Park KH, Cho YS. Origin of high piezoelectricity of inorganic halide perovskite thin films and their electromechanical energy-harvesting and physiological current-sensing characteristics. *Energy Environ Sci* 2020;13:2077-86. DOI
29. He F, Lin K, Shi D, et al. Preparation of organosilicate/PVDF composites with enhanced piezoelectricity and pyroelectricity by stretching. *Compos Sci Technol* 2016;137:138-47. DOI
30. Brennan MC, Herr JE, Nguyen-Beck TS, et al. Origin of the size-dependent stokes shift in $CsPbBr_3$ perovskite nanocrystals. *J Am Chem Soc* 2017;139:12201-8. DOI PubMed
31. Huang C, Wang Y, Cheng Z, Wu Y, Li J, Deng Y. Dielectric screening enabled ultrastable luminescence in $CsPbBr_3$ perovskite crystal encapsulated by ferroelectric Poly(vinylidene fluoride). *Chem Eng J* 2020;401:126120. DOI
32. Ippili S, Jella V, Eom J, et al. An eco-friendly flexible piezoelectric energy harvester that delivers high output performance is based on lead-free $MASnI_3$ films and $MASnI_3$-PVDF composite films. *Nano Energy* 2019;57:911-23. DOI
33. Pandey R, Sb G, Grover S, et al. Microscopic origin of piezoelectricity in lead-free halide perovskite: application in nanogenerator design. *ACS Energy Lett* 2019;4:1004-11. DOI
34. Sultana A, Ghosh SK, Alam MM, et al. Methylammonium lead iodide incorporated poly(vinylidene fluoride) nanofibers for flexible piezoelectric-pyroelectric nanogenerator. *ACS Appl Mater Interfaces* 2019;11:27279-87. DOI PubMed
35. Ippili S, Jella V, Eom S, Hong S, Yoon SG. Light-driven piezo- and triboelectricity in organic-Inorganic metal trihalide perovskite toward mechanical energy harvesting and self-powered sensor application. *ACS Appl Mater Interfaces* 2020;12:50472-83. DOI PubMed
36. Khan AA, Rana MM, Huang G, et al. Maximizing piezoelectricity by self-assembled highly porous perovskite-polymer composite films to enable the internet of things. *J Mater Chem A* 2020;8:13619-29. DOI
37. Mondal S, Paul T, Maiti S, Das BK, Chattopadhyay KK. Human motion interactive mechanical energy harvester based on all inorganic perovskite-PVDF. *Nano Energy* 2020;74:104870. DOI
38. Rodriguez BJ, Callahan C, Kalinin SV, Proksch R. Dual-frequency resonance-tracking atomic force microscopy. *Nanotechnology* 2007;18:475504. DOI